Electrical Modulation of Ion Concentration in Dual-Gated Nanochannels

Yang Liu, Qiushi Ran, and Robert W. Dutton

Center for Integrated Systems, Stanford University,
Stanford, CA 94305, U.S.A.
Phone: (650)723-9796, E-mail: yangliu@gloworm.stanford.edu

Abstract

Coupled Poisson-Nernst-Planck and Stokes simulations demonstrate the operating principles of using electrical biases in dual-gated nano-fluidic channels to create localized and tunable solution zones of either depleted or accumulated ions. Scaling studies reveal that such ion modulations overcome the limit of counter-ion screening and remain effective even for channel widths greatly exceeding the Debye screening length. The underlying mechanism is attributed to the transport-induced de-screening of gating potentials.

Introduction

Sample preparation plays an essential role in analytical chemistry and bio-medical diagnostics, for which a broad spectrum of micro- and nano-fluidic techniques have been developed, including isotachophoresis [1], field amplified sample stacking [2], and electro-kinetic trapping [3]. Particularly for point-of-care bio-medical devices, the integration of biological sample preparation processes remains a key challenge [4]. To address such challenges, research interest has recently been focused on nano-fluidic "transistors", which manipulate the transport of ions and molecules via field-effect gating using surface charges [5,6] or gate electrodes [7-10]. Other potential applications range from fuel cells [11] to desalination [12]. Nevertheless, in contrast to semiconductors, ionic solutions are zero-bandgap conductors. Therefore, the distance of electrostatic gating is commonly limited by the screening of mobile counter-ions, as characterized by the Debye screening length, Λ_D (~0.8 nm for 150 mM ionic strength). This imposes a stringent constraint on device fabrication and system integration, considering that many important applications involve high ionic concentrations, e.g. bio-sensing under physiological condition (150 mM) or desalination of seawater (500 mM) and brackish water (10~500 mM). Additionally, clogging causes a more serious problem for small ion channels.

In previous work, a transport-induced de-screening effect was exploited to overcome the screening limit in nanowire and nanopore biosensor devices [13,14]. It was further revealed that the de-screening applies to field-effect gated nanochannels in general [9,10]. In this work, the operating principles and scaling behavior are studied for a novel type of nano-fluidic device employing dual-gated nanochannels, particularly those with widths greatly exceeding Λ_D. The essential idea is to exploit de-screening for highly efficient, electrically-tunable ion modulation.

Device Structure and Model

The top half of the basic device structure is shown in Fig. 1, where a 50 nm wide nano-channel connects two solution reservoirs. Two pairs of gate electrodes are embedded at channel sides to control electrostatics and create an ion modulation zone between them. Two additional solution electrodes are placed at the reservoir boundaries. An external bias V_d is applied between them to drive electro-kinetic transport in the longitudinal direction. The model equations and boundary conditions are described in Table 1. The ion transport within the channel and reservoirs is modeled by Poisson-Nernst-Planck (PNP) equations including advection. The transport of an incompressible, Newtonian fluid that has a low Reynolds-number is modeled by Stokes-divergence equation. The ion osmotic pressure is explicitly treated to maintain consistency with the Scharfetter-Gummel method in PNP and improves numerical convergence. The no-slip boundary condition is proper for the hydrophilic channel walls assumed in this study, for which the complication of hydrodynamic slippage is insignificant [15]. The Poisson equation is applied to the oxide region. It is assumed that the solution pH is adjusted to the isoelectric point, so that the fixed oxide surface charge is negligible. All the above modeling equations are self-consistently solved using a general purpose device simulator [16].

Simulation Results and Discussions

As shown in Fig. 2, we study four electrical biasing schemes that are categorized into three operation modes: no gating (A), depletion (B), and accumulation (C & D). Simulated potential profiles along the symmetry line (y=0) are shown in Fig. 3 for all bias schemes. The forward biasing (Scheme B) modulates channel electrostatics so that potential drop occurs predominantly in the zone between the gates. In contrast, the

grounded-gate biasing (Scheme C) tends to hold the potential flat within the zone; this tendency is further enhanced by reverse biasing (Scheme D). Due to ionic flux continuity, such modulations on channel electrostatics directly result in changes in ion concentration. As observed in Fig. 4, the ion depletion (accumulation) occurs within the central zone, corresponding to high (low) electrical field strength therein. Further simulations for various ionic strengths (C_0) and V_d's show a scaling trend in Fig. 5, where the normalized ion concentration at the center (x=y=0 in Fig. 1) is used to represent the modulation level. Both the depletion and accumulation levels become more significant at higher V_d and lower C_0. Particularly for a V_d of 6 V, the ion depletion (accumulation) is 6X (3X) for 150 mM ionic strength, i.e. the physiological condition. The modulation level is further enhanced to 25X (8X) for 15 mM ionic strength. Remarkably, such modulations are achieved where the channel width (50 nm) corresponds to ~$20\Lambda_D$ for 15 mM case and ~$60\Lambda_D$ for 150 mM case. The fluid velocity profiles are visualized in Fig. 6. For the control Scheme A, an insignificant entrance effect is observed at the channel openings. For the other three schemes, strong fluid vortices are observed at the edges of the gate electrodes. The rotation directions of the depletion and accumulation modes are opposite. Such vortices originate from induced electro-osmosis and are explained by symmetry properties of the electrical biasing [9].

The key question to answer in understanding the device physics is how the gating potentials can effectively control the channel electrostatics, even though the channel width is ~$60\Lambda_D$? This is further investigated in Fig. 7(a), where the potential difference between the case without gating and that with fixed gating (V_{g1}=+3 V and V_{g2}=-3V) is shown for different V_d's. For V_d=0 V, the extensions of gating potentials are completely limited at the gate surfaces, obeying the Debye screening behavior. However, as V_d increases and ion transport becomes stronger, the screening effect is significantly suppressed, leading to greatly extended gating potentials. The trend of transport-induced de-screening is clearly observed in Fig. 7(b), where $\Delta\psi_m$, the maximum potential change along the central line (y=0), is shown to increase with V_d for both cases of 15 mM and 150 mM ionic strengths.

It is highly desirable to have large ion modulation zones for practical applications. The zone size is determined by the gate electrode spacing, L_S, the scaling of which is shown in Fig. 8. In the depletion mode, the modulation level decreases linearly with increasing L_S for a fixed V_d. This is expected from the reduced amplification of the electric field in the central zone. On the other hand, in the accumulation mode, the dependence on L_S is rather small. In this mode, the potential is held flat in the central zone and thus insensitive to L_S variations. Practically, it is important to extract the depleted or accumulated solution out of the central zone. We further study a device with side channels to demonstrate such a possibility (Fig. 9a). In this case, negative pressure difference is applied at the outlet for a pressure-driven flow. Using the depletion mode for example, the depleted solution is extracted at the outlet for a moderate pressure difference of 15 kPa (Fig. 9b). The fluid velocity pattern in the side channel is shown in Fig. 9c. Besides an initial entrance effect, a parabolic pattern that is characteristic of pressure-driven flow is developed toward the outlet. It is noted that other cross-flow designs may be more efficient to extract the solutions than the one demonstrated here as an example. Furthermore, multi-stage systems can be designed to achieve a multiplication of the ionic modulation capabilities.

Summary

Coupled ion and fluid transport models have been developed to study the operating principles and scaling behavior of dual-gated nanochannels. Various biasing schemes have been demonstrated to achieve efficient and localized ion modulation. Owing to the transport-induced de-screening effects, such modulations overcome the Debye screening limit, offering an electrically-tunable mechanism for sample preparation and water treatment.

Acknowledgement

We appreciate discussions with Dr. Connor Rafferty on model numerical implementation.

References

[1] B. Jung, R. Bharadwaj and J. Santiago, *Anal. Chem.* vol.78, p.2319, 2006
[2] R.-L. Chien and D. Burgi, *Anal. Chem.* vol. 64, p.1046, 1992
[3] Y.-C. Wang, A. Stevens, and J. Han, *Anal. Chem.,* vol. 77, p.4293, 2005
[4] J. Chabbal, *IEDM Tech. Dig.,* p.15, 2009;
[5] H. Daiguji, Y. Oka, and K. Shirono, *Nano Lett.* vol. 5, p.2274, 2005;
[6] E. Kalman, I. Vlassiouk, and Z. Siwy, *Adv. Mater.* vol. 20, p.293, 2008;
[7] R. Karnik, et al. *Nano Lett.* vol. 5, p.943, 2005;
[8] K. Chun et al. *Chem. Phys. Lett.* vol. 418, p.561, 2006;
[9] Y. Liu, D. Huber and R. Dutton, *Appl. Phys. Lett.,* vol.96 p.253108, 2010;
[10] Y. Liu et al., *Appl. Phys. Lett.*, in press
[11] R. Fan, et al. *Nat. Mater.* vol. 7, p.303, 2008;
[12] S.J. Kim et al. *Nat. Nanotech.* vol. 5, p.297, 2010;
[13] Y. Liu et al. *IEDM Tech. Dig.* p. 491, 2008;
[14] Y. Liu, J. Sauer, and R. Dutton, *J. Appl. Phys*. vol. 103, p.084701, 2008;
[15] C. Bouzigues et al. *Phys. Rev. Lett.,* vol. 101, p.114503, 2008;
[16] http://www-tcad.stanford.edu/~prophet

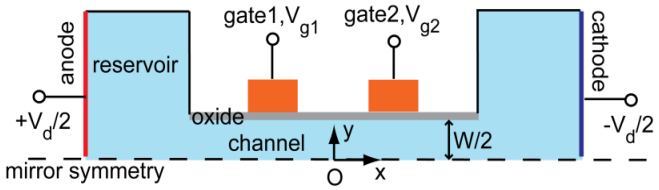

Fig. 1: Schematic plot of the top half of a dual-gated nanochannel device (not to scale). The nominal channel width W=50 nm and length 1.4 μm; gate electrode length and their spacing 200 nm each; gate to channel oxide thickness 2 nm; reservoir width and length 1 μm each.

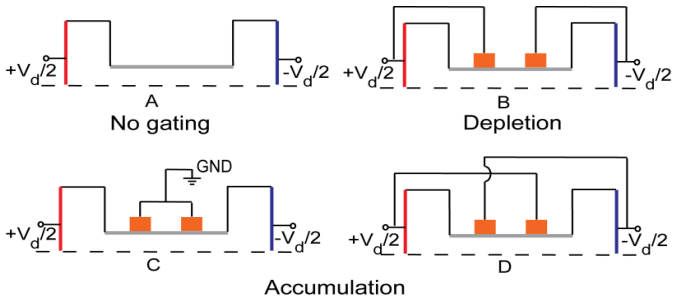

Fig. 2: Four biasing schemes for three operation modes. A is a control without gates. B forwardly biases the dual gates for ion depletion operation. C ties both gates to ground, and D reversely biases the gates. Both C and D are for ion accumulation operation. An external bias V_d is always applied between cathode and anode.

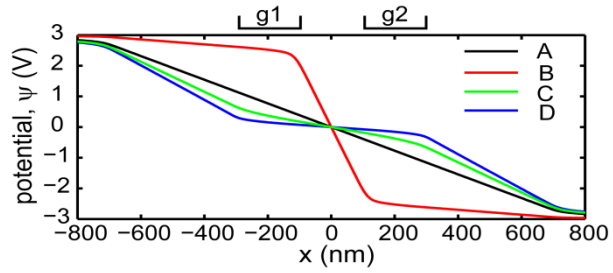

Fig. 3: Simulated potential profiles along the central symmetry line for the four biasing schemes in Fig. 2. Ionic strength C_0 is 15 mM (Λ_D~2.5 nm); V_d is 6 V. Only the portion of interest is shown.

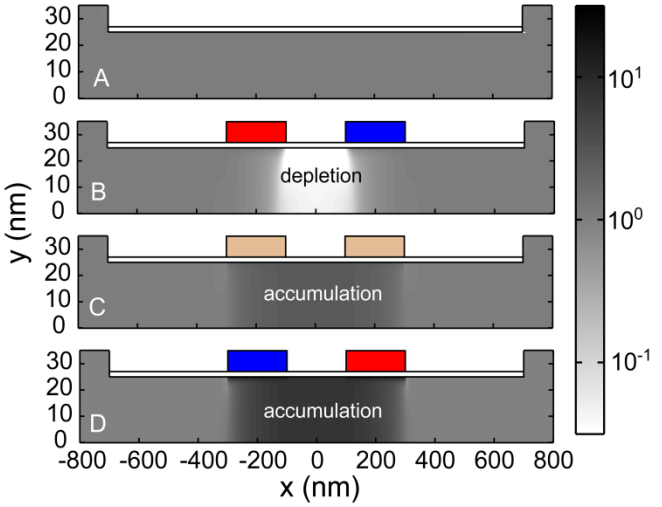

Fig. 4: 2-D profiles of nomalized ion concentration, $\bar{C} = {(C_+ + C_-)}/{2C_0}$, for the four biasing schemes. Conditions are the same as Fig. 3. The intensity is in log scale. Only the portion of interst is shown.

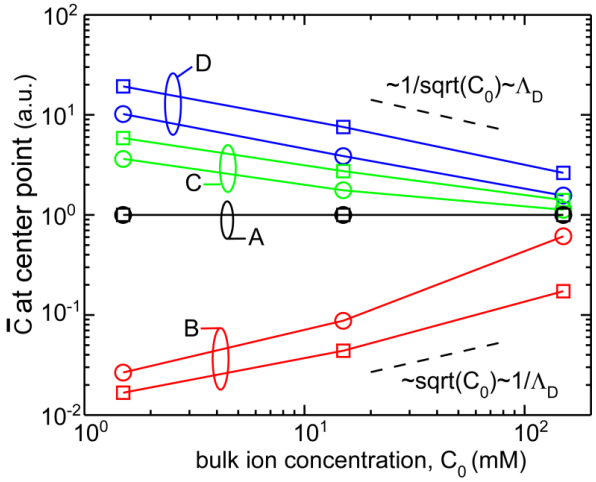

Fig. 5: Normalized ion concentration, $\bar{C}$, at the center point (x=y=0 in Fig. 1) vs. bulk ionic strength, C_0, for the four biasing schemes. Two V_d values are used: 3 V (circles) and 6 V (squares).

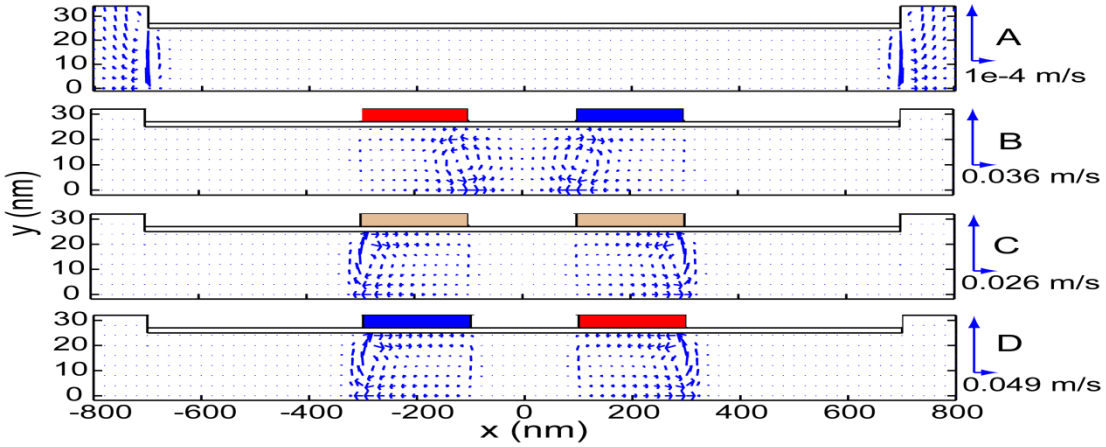

Fig. 6: Vector plots of fluid velocity for the four biasing schemes. Conditions are the same as Fig. 3. Velocity scale references are given for both longitudinal and transverse directions in each sub-figure. Only the portion of interest is shown.

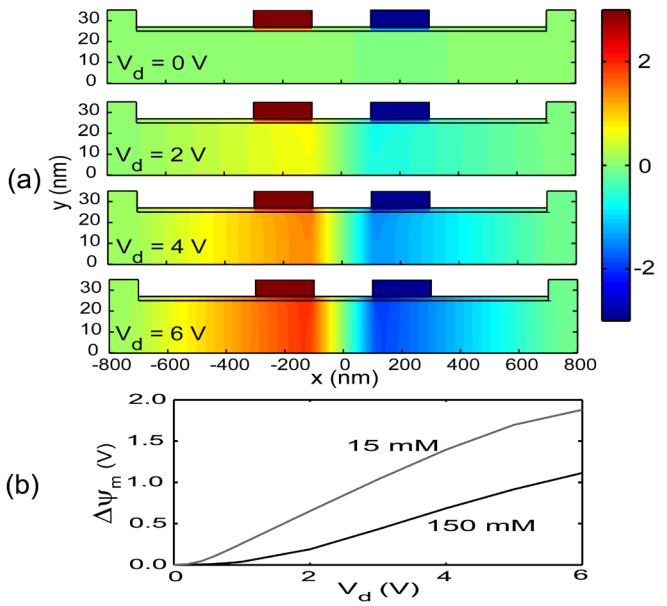

Fig. 7: (a) potential difference induced by fixed gating potentials (V_{g1}=+3 V and V_{g2}= -3 V) for different V_d biases. C_0 is 15 mM; (b) maximum potential difference along the central symmetry line ($\Delta\psi_m$) vs. V_d biases for two C_0 values: 15 mM and 150 mM.

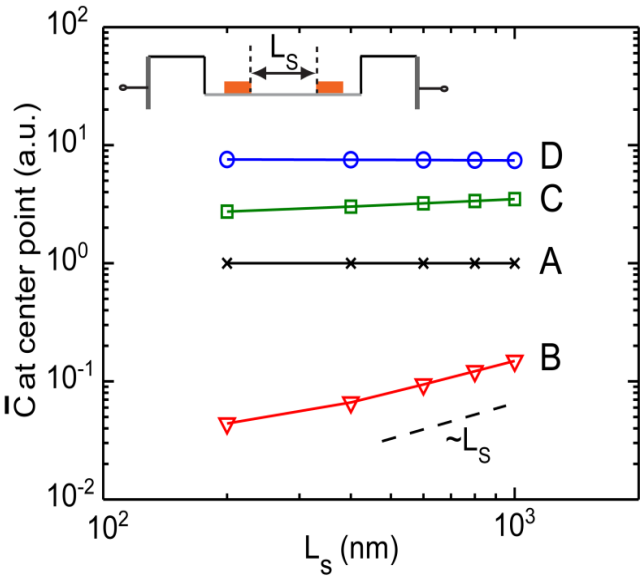

Fig. 8: Normalized ion concentration, $\bar{C}$, at center point (x=y=0 in Fig. 1) vs. spacing between the two gate electrodes, L_S, for the four biasing schemes in Fig. 2. C_0 is 15 mM, and V_d is 6 V.

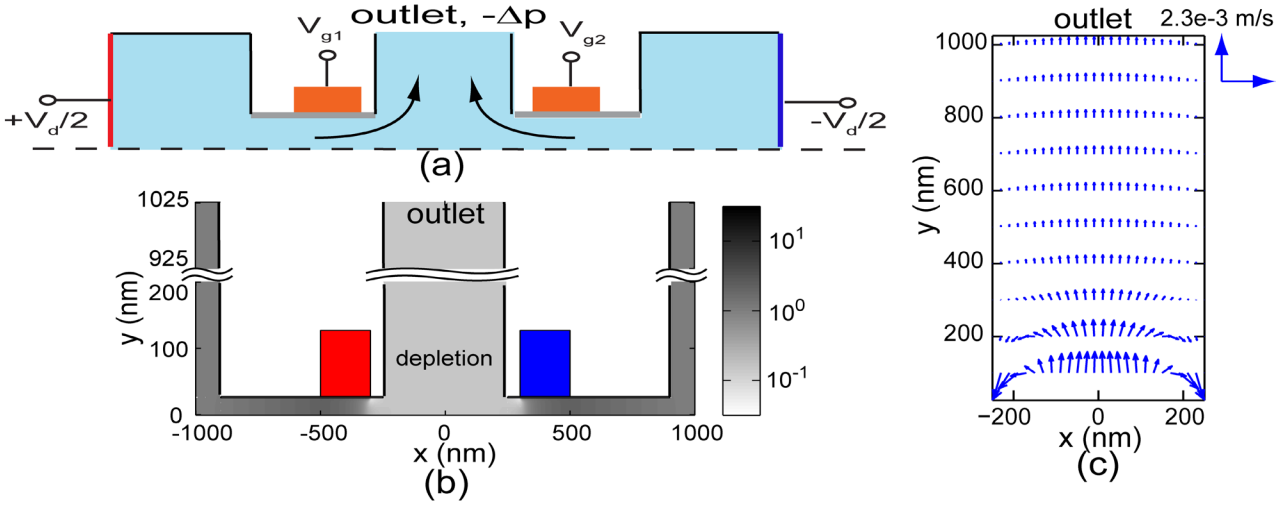

Fig. 9: (a) The top half of a device with side channels. Negative pressure difference is applied at the outlet boundary to extract out the modulated solution; (b) simulated profile of $\bar{C}$ under depletion mode operation (scheme B). Only the portion of interest is shown. C_0=15 mM, V_d=6 V, L_S=600 nm, and Δp=15 kPa; (c) simulated fluid velocity pattern, where only the side channel portion is shown.

Table 1: Model equations in this study. PNP boundary conditions include: Dirichlet conditions for potential and ion concentration at reservoir cathode/anode; Neumann conditions with zero normal fluxes for symmetry axis, oxide walls and other simulation domain boundaries. Stokes boundary conditions include: no-slip for channel walls; slip with zero normal velocity for the symmetry axis; zero pressure and zero gradient of normal velocity at reservoir boundaries.

Cations and Anions (PNP)	Fluid (Stokes-Divergence)	Gate Oxide (Poisson)
$\nabla\cdot(\varepsilon_w\nabla\psi)+q(C_+-C_-)=0;$ $q\nabla\cdot(-D_+\nabla C_+-\mu_+C_+\nabla\psi+C_+\vec{u})=0;$ $-q\nabla\cdot(-D_-\nabla C_-+\mu_-C_-\nabla\psi+C_-\vec{u})=0.$ C_+/C-: cation/anion concentration; ε_w: $80\varepsilon_0$; μ_+ and μ_-: 7.62e-8 m^2/Vs; D: $\mu k_BT/q$.	$-\nabla p'+\gamma\Delta\vec{u}-q(C_+-C_-)\nabla\psi-$ $k_BT\nabla(C_++C_-)=0;$ $\nabla\cdot\vec{u}=0;\quad p=p'+k_BT(C_++C_-).$ $\vec{u}$: solvent velocity vector; p: solvent pressure; γ: viscosity, 0.001 Ns/m^2 for water.	$\nabla\cdot(\varepsilon_{ox}\nabla\psi)=0;$ ε_{ox}: $3.9\varepsilon_0$. **Gate Electrode** Constant potential: $\psi=V_{g1}$ or V_{g2}